DOI: 10.31276/VJSTE.2024.0014

A geometrical optimisation of a coplanar micro-electrode structure for microfluidic flow cytometry

Van Phu Nguyen[1], Van-Anh Bui[1], Thu Hang Nguyen[2], Trung Kien Do[1], Van Thanh Pham[1], Thi Thanh Thuy Dang[1], Quang Loc Do[1*]

[1]*Faculty of Physics, University of Science, Vietnam National University - Hanoi, 334 Nguyen Trai Street, Thanh Xuan Trung Ward, Thanh Xuan District, Hanoi, Vietnam*
[2]*Faculty of Electronics and Telecommunications, University of Engineering and Technology, Vietnam National University - Hanoi, 144 Xuan Thuy Street, Dich Vong Hau Ward, Cau Giay District, Hanoi, Vietnam*

Received 1 February 2024; revised 7 March 2024; accepted 8 May 2024

Abstract:

Single-cell analysis provides a more information-rich approach to disease diagnosis than traditional methods. At the cellular level, electrical properties have been established as reliable disease markers, capable of revealing variations between individual cells. This study focuses on optimising the geometry of a coplanar micro-electrode structure for detecting human lung adenocarcinoma cells (A549) within a fluid channel using impedance flow cytometry. A549 cells were chosen due to their frequent occurrence in cancer cases and the extensive documentation of their electrical properties and size. To further investigate the electric field and optimise the electrode design for single-cell detection, a numerical 3D model based on the finite element method (FEM) was developed and implemented. The functionality of the sensing structure was validated using COMSOL Multiphysics, with the Electric Current module defining scalar electric potential within the 3D model. Simulations explored various parameters, including electrode dimensions, frequency range, object sizes, and electrical conductivity, to fine-tune the sensor's performance. Additionally, the study elucidates the impact of cell position within the channel structure and cell size on impedance measurements. This numerical investigation provides insights into the acquired impedance signals, contributing to the optimisation and standardisation of the device. The proposed sensor system holds significant potential across various applications in biomedicine and chemistry, particularly in point-of-care scenarios, where the sensor chip can be conveniently configured for measurements and discarded after use.

Keywords: **cell detection, impedance flow cytometry, microfluidic system, reactance, resistance.**

Classification numbers: **2.1, 2.3, 3.2**

1. Introduction

Cancer remains the leading cause of mortality in both developed and developing nations [1]. Among the primary causes of cancer-related deaths is lung cancer [2]. Currently, lung cancer diagnosis predominantly relies on a combination of medical imaging and invasive biopsies for histopathological confirmation [3]. However, these methods possess several drawbacks, such as requiring highly trained personnel, confirmation times of approximately 48 hours per sample, and a lack of ongoing monitoring [4]. Additionally, these modalities often have limited capability to assess phenotypic changes associated with chemoresistance and biomarkers. Cancer progression is closely linked to changes in the number of cancer cells present in the blood, particularly in cases of metastasis, which necessitates the development of mobile cancer cell counting systems that enable rapid, low-cost testing, requiring minimal sample sizes and analysis time.

In recent decades, impedance flow cytometry (IFC) has emerged as an efficient method for single-cell analysis [5-8]. This technique also provides additional cell information through non-invasive, label-free impedance measurements, offering applications ranging from single-cell counting to point-of-care diagnosis [9-13]. However, one of its main limitations is the variability of the signal impedance with the cell's position in the sensing region. This method has also been applied to analyse single cells in controlled oxygen microenvironments to study cellular responses to hypoxia [14-16]. The position-dependent impedance signal poses a challenge to the accuracy of IFC. Furthermore, the electrode configuration influences both the electric field distribution and impedance, considering shape and size. Variations in impedance signals as cells pass through the sensing area allow for the extraction of data about the size, shape, and dielectric properties of these cells [17]. The dimensions of the channel and micro-electrodes are typically selected

*Corresponding author: Email: locdq@hus.edu.vn

based on experimental correlation with the micro-object of interest. Several previous studies have employed impedance analysis to investigate parameter influence and optimise channel structure [18-23]. However, the analysis of both resistance and reactance components has not been widely explored recently. Additionally, most studies of single-cell analysis using the IFC method have focused on single-frequency analyses, neglecting the reactance component and excitation frequency optimisation.

A previous study introduced a novel impedance analysis technique, which includes the assessment of both resistance and reactance [24]. This study presents an effective methodology for the detection and quantification of human lung cells (A549) using complex impedance analysis within an impedance-based microfluidic (IFC) device. This approach provides additional insights into the electrical characteristics of cells within the microfluidic channel, facilitating the differentiation of various cell types in the fluidic system. The detection and quantification capabilities were simulated using COMSOL Multiphysics. This model is optimised to identify the most effective structure and stimulation frequency for biological cell sizes. The numerical analysis enhances the accuracy, improving the specificity and sensitivity of conventional impedance sensing structures. This innovative approach lays the groundwork for developing Lab-on-a-Chip (LoC) devices, poised for future biomedical applications. By harnessing the capabilities of complex impedance analysis in microfluidic systems, these devices hold the potential to revolutionise diagnostics, research, and biomedical applications by offering advanced tools for detecting and analysing specific cell types.

2. Materials and methods

2.1. Sensor design

Figure 1 presents the proposed complex impedance-based biosensor structure. The microfluidic chip consists of a symmetrical channel structure with a length of 1,000 μm, a width of 50 μm, a height of 50 μm, and a sensing electrode area of 50 μm in length and 30 μm in width.

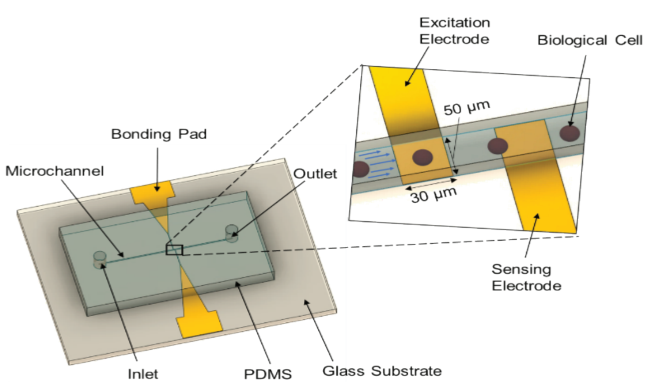

Fig. 1. 3D visualisation of the proposed complex impedance analysis sensor structure.

The selection of the microfluidic chip size is critical, as clogging may occur if the channel is too small, while a significant decrease in sensitivity could result if the channel is too large. The dimensions chosen in this manuscript are based on commonly used sizes in recent experimental studies within the biomicrofluidics field, and are deemed suitable to meet these requirements. Similar channel dimensions have been utilised in previous studies for cancer cell detection experiments [25, 26].

2.2. Single sphere modelling

For cell impedance evaluation, a frequency-dependent voltage is applied to the system containing the cell in suspension, and the electrical current response of the system is measured. The electrical impedance of the system $\tilde{Z}(j\omega)$ is defined as the ratio of the voltage $\tilde{U}(j\omega)$ and current response $\tilde{I}(j\omega)$.

$$\tilde{Z}(j\omega) = \frac{\tilde{U}(j\omega)}{\tilde{I}(j\omega)} = R + jX \quad (1)$$

where $J = \sqrt{-1}$ and ω is the frequency. The biological impedance is a complex number with resistance (R) as the real part and reactance (X) as the imaginary part, both expressed in Ω, respectively.

Impedance signals indicate which cells are collected when an A549 cell passes through the electrode sensing area. In this simulation, an alternating current signal is applied, and a single-sphere spherical suspension cell model is used for cell modelling to collect detailed information about the cell. The modelled A549 cell was assumed as a single sphere of 7.5-μm radius, with dielectric permittivity (ε_r) of $60\varepsilon_0$ and electrical conductivity (σ_r) of 1.05 S/m [27, 28], and was suspended in a sucrose solution medium (ε_r=78; σ=1.76×10^{-3} S/m). Sucrose plays a vital role in maintaining the osmotic potential and preserving water within cells. Furthermore, it has been utilized as a buffer solution in microchannels, with some studies employing an 8.6% sucrose solution for this purpose [29].

Regarding the influence of cell membranes, certain studies have demonstrated that the cell membrane acts as a strong electrical insulator, with cells behaving like insulating particles at low frequencies [30-32]. However, research findings indicate that minor membrane conductivities exert little influence on impedance data, while larger conductivities lead to the dominance of the cell's dielectric properties by internal factors, notably those linked to the nucleus [33]. Consequently, this study employs a single-sphere model for analysis. For a simplified system analysis, an equivalent circuit model is often utilised, with such an approach developed by K.R. Foster, et al. (1989) [34].

3. Numerical simulation

To explore the electric field and determine the conductance of specific biological entities, a three-dimensional model employing the finite element method (FEM) was developed. This model was designed and analysed using COMSOL Multiphysics 6.0 software from COMSOL Inc., headquartered in Stockholm, Sweden. The software excels in simulating electrical components, including conductivity and permittivity, as well as devices used in electrostatic, magnetic static, and electromagnetic quasistatic applications. Special attention is given to capturing the influence of various physical characteristics. In this study, the biological cell, assumed to have no deformation, is represented as a single-sphere model within the simulation [35].

Biological cells in the fluid stream are identified based on changes in impedance between two sensing electrodes. Impedance values for the stimulating and sensing electrodes were assessed according to the specific position of the moving cell within the microchannel, and the differences between these values were evaluated. In this simulation, the stimulating electrode is consistently maintained at a voltage of 1 V, while the sensing electrode remains at 0 V. Consequently, the relative impedance of the electrode structure can be modulated by the current flowing between the electrode pairs.

In the steady state, the electrostatic current in the conductive medium is regulated by the static continuity equation as follows:

$$\nabla \cdot J = Q_{(j,v)} \tag{2}$$

In a static scenario, the potential relationship V is established as follows:

$$E = -\nabla V \ (V/m) \tag{3}$$

Here, E represents the gradient of the electric potential V, analogous to the classical gravitational field. The electric isolation node serves as the default boundary condition, implying that no current enters the boundary.

$$n \cdot J = 0 \tag{4}$$

At this boundary, the absence of current flow is enforced. This condition is particularly relevant at symmetric boundaries where the potential is recognised to exhibit symmetry about the boundary. Importantly, the default insulation condition is not imposed on the internal boundary.

The outside environment was filled with air. Table 1 lists the material properties used in the numerical calculation [36]. Fig. 2 shows the mesh of the proposed complex impedance sensing structure, which is denser in the important elements, including cells and electrodes while remaining less dense in other areas to optimize the resources.

Table 1. Parameters of materials used in simulations [36].

Material	Permittivity	Conductivity (S/m)
Air	1	10^{-15}
Polydimethylsiloxane (PDMS)	2.75	4×10^{-15}
Glass	5.5	10^{-15}
A549 cell	60	1.05
8.6% sucrose solution	78	1.76×10^{-3}

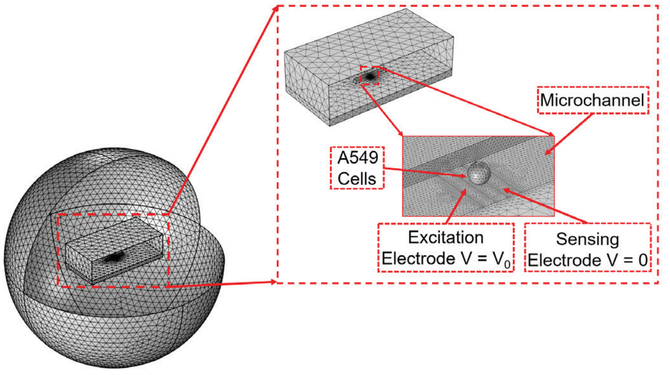

Fig. 2. Simulated A549 cells.

4. Results and discussion

4.1. The electric field distribution of the sensor

Figure 3 illustrates the electric field distribution within the sensor structure, depicting the electric field intensity that extends beyond the air, encompassing the space between the stimulating and sensing electrodes.

The visualisation demonstrates the reach and coverage of the electric field, highlighting its presence and influence over the specified region within the sensor structure. This comprehensive depiction provides insights into the spatial characteristics and extent of the electric field, offering a

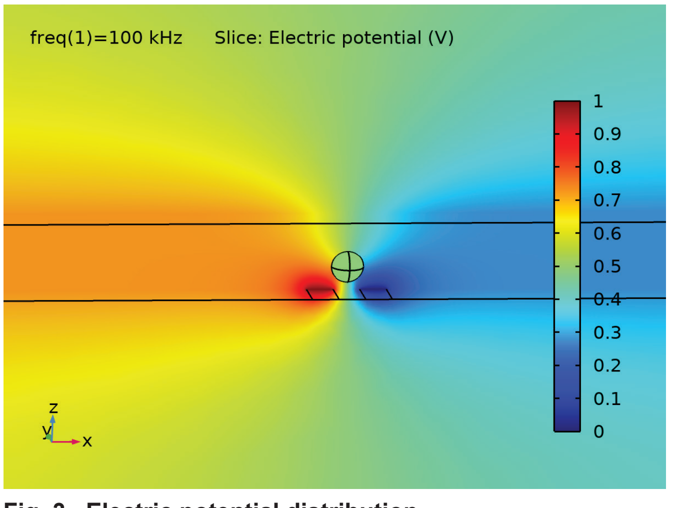

Fig. 3. Electric potential distribution.

better understanding of how it interacts with the surrounding environment and potential targets, such as biological cells within the fluid stream.

4.2. Detection of A549 cells inside the microfluidic channel

The impedance change ΔZ is given by the difference between the impedance Z_A received when the A549 cell passes through the sensing structure in the sucrose 8.6% solution and the impedance Z_B obtained in the absence of the A549 cell in the Sucrose 8.6% solution channel:

$$|\Delta Z|=|Z_A-Z_B| \tag{5}$$

The impedance change due to the passage of the A549 cell through the sensing area in the real part is ΔR, also known as resistance change, while the change in the imaginary part ΔX is known as reactance change. The simulation results illustrate the correlation between the impedance change and the position of the A549 cell within the sucrose 8.6% solution channel (Fig. 4). Notably, the impedance signal shows distinct peaks as the A549 cell enters the region between the two electrodes.

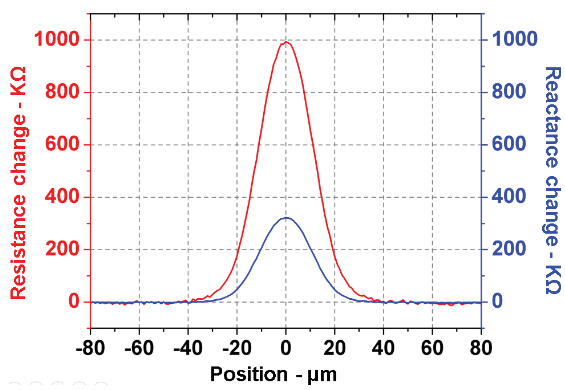

Fig. 4. Simulation results: A typical signal with a 7.5 μm radius A549 cell moves through the sensing area in the 8.6% Sucrose solution channel.

In this analysis, the frequency domain of the electric current module in a simulation model was employed to scrutinise the complex impedance of the sensor under an excitation signal frequency of 100 kHz. As depicted in Fig. 4, the simulation results reveal maximum changes in resistance and reactance of approximately 1,000 kΩ and 325 kΩ, respectively. These variations are observed as the simulated A549 cell, with a radius of 7.5 μm, traverses the sensing electrode structure within the 8.6% sucrose solution channel.

This simulation provides valuable insights into the dynamic response of the sensor under specific frequency conditions, demonstrating substantial changes in both resistance and reactance parameters. Understanding these impedance variations, particularly in response to cell movement, contributes to a more comprehensive understanding of the sensor's behaviour and aids in refining the design for optimal performance. The observed changes underscore the sensor's sensitivity to the presence of cells, further emphasising the potential utility of this technology for precise cell detection applications within microfluidic environments.

4.3. Impact of A549 cell size on impedance signal

Figure 5 illustrates the relationship between impedance change and the radius of cells passing through the sensing area. In order to examine impedance changes concerning A549 cells of different radii moving through the sensor channel, simulations were conducted with cell radii ranging from 2 to 10 μm. Notably, the impedance change becomes more pronounced as larger A549 cells pass through the sensing region. At the 0 mm position, located between the two electrodes, the most significant impedance change corresponds to a cell radius of 7.5 μm, is evident. These results were obtained by varying the excitation frequency from 10 kHz to 10 MHz. Numerical calculations reveal a proportional relationship between the change in impedance and the increase in cell radius.

(A)

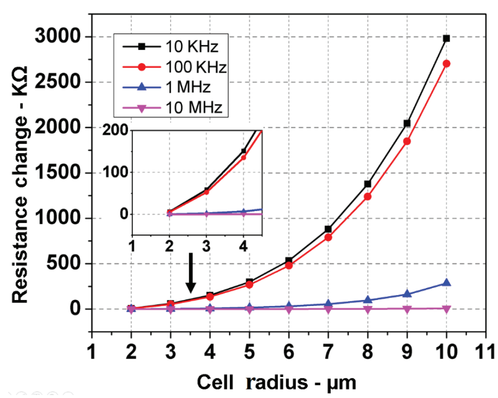

(B)

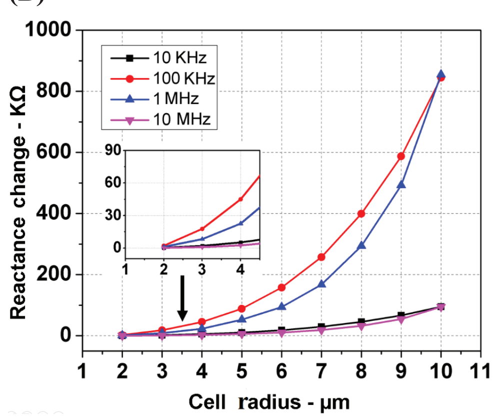

Fig. 5. The dependence of (A) resistance change and (B) reactance change on A549 cell size in fluidic channel structure.

Moreover, only marginal impedance changes are observed as the cell size decreases. The inset demonstrates the simulation results for cell radii ranging from 2 to 4 μm to explore impedance variations in instances where the cell size is small. The results show that the change in resistance varies up to approximately 150 KΩ while the reactance exhibits a maximum change of about 22.6 KΩ. Additionally, the simulation results show that the change in impedance and reactance due to cell size is negligible at low frequencies. However, significant changes are observed at higher frequencies (10 MHz). This marked variation may be associated with changes in the cell membrane and electrical double layer, which behave like a capacitor. As a result, the capacitance of C_{mem} and C_{dl} change depending on the applied AC frequency (ω).

In the lower frequency range (ω<1 MHz), the electrical double layer primarily influences the system impedance, resulting in low sensitivity for cell detection. As the frequency increases (1<ω<10 MHz), the capacitance of the electrical double layer gradually diminishes, and the system impedance is determined by the size of the cell. T. Sun, et al. (2010) [27] introduced a comprehensive equivalent circuit model for a cell, incorporating membrane resistance and cytoplasmic capacitance. Their previous research [27] extensively discussed the methodology for calculating the values of R_i, C_i, R_{mem}, and C_{mem} in this model.

Hence, the results demonstrate that the impedance undergoes a notable change in both the resistance and reactance components when large A549 cells pass through. Moreover, variations in cell sizes and electrical characteristics across different cell types make it possible to distinguish between them by analysing changes in impedance, encompassing both resistance and reactance.

However, Fig. 5 in this study depicts the relationship between changes in resistance and reactance relative to the cell's radius, rather than focusing on impedance variation. This research specifically examined the relationship between impedance changes and cell radius, as shown in Fig. 6. The results indicate that the sensitivity of electrical impedance to particle size tends to be more pronounced at lower frequencies compared to higher frequencies, consistent with theoretical expectations. Moreover, the relationship between frequency and changes in resistance and impedance. Importantly, the results highlight that reactance alterations do not follow the same trend as resistance. This approach offers a more comprehensive understanding of the electrical properties unique to each cell.

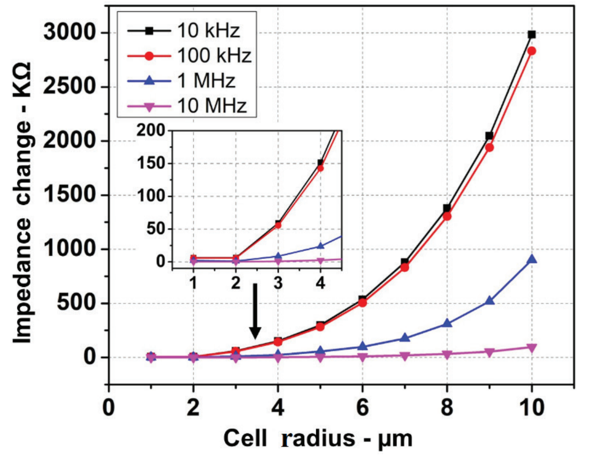

Fig. 6. The dependence of impedance change on A549 cell size in fluidic channel structure.

4.4. Influence of cell vertical position on impedance signal

In recent years, various impedance flow cytometry methods have been developed for biomedical applications, ranging from blood cell quantification for disease diagnosis to microbiological studies and monitoring cell phenotype changes.

However, a significant challenge to the accuracy of impedance sensing technology is its dependency on the position of objects within the channel. As a result, acquired impedance signals can vary, affecting the sensor's sensitivity when objects pass through the sensor area along different trajectories. Numerous technical advancements have been introduced to improve the precision of impedance-based tests. These include approaches such as controlling cell positions in microfluidic channels [37], signal processing [38], and designing specific electrode configurations [39].

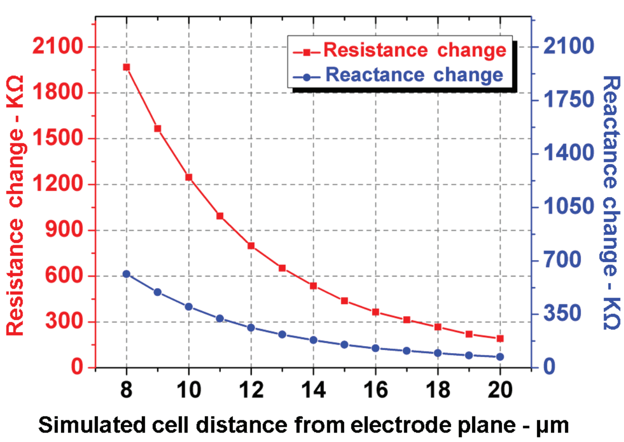

Fig. 7. Simulated impedance changes according to the vertical position.

To further investigate these phenomena, this study conducted an analysis of impedance signals by varying the position of the A549 cell within the channel, ranging from 8 to 20 µm away from the electrode plane. The survey frequency was held constant at 100 kHz, and an 8.6% sucrose solution was used. Fig. 7 visually illustrates the dependency of impedance changes on the cell's location in the sensing region. The resistance exhibited an approximate change of 2,000 KΩ, while the reactance shifted by around 610 KΩ. Importantly, the impedance changes in impedance sensing demonstrate an inverse relationship with the distance between the simulated cell and the electrode plane. Therefore, to enhance the sensitivity of the microsensor, reducing the cell-to-electrode surface height to match typical cell sizes becomes crucial.

4.5. Influence of electrode size, the distance between two electrodes on impedance signal

This study examines the impact of coplanar electrode dimensions to enhance the sensitivity of impedance flow cytometry. The standard setup includes two coplanar electrodes with a width equal to the spacing between them.

In this research, numerical calculations were performed using electrodes of uniform size, with distances ranging from 5 to 50 µm. The cell-to-surface distance was consistently set at 11 µm, with the cell positioned between two electrodes. Fig. 8 depicts the impedance values obtained as a simulated cell traversed between the excitation and sensing electrodes in an 8.6% sucrose solution. The results indicate that the most significant impedance change occurs when the electrode size and spacing are within the 10 to 15 µm range, resulting in a resistance change of 1,000 KΩ and a reactance change of 340 KΩ.

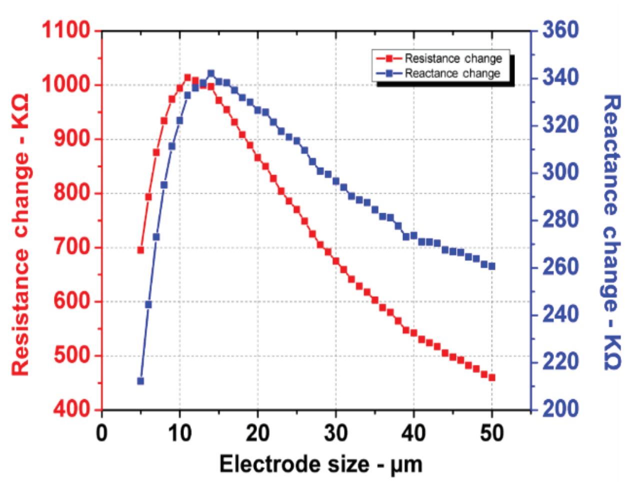

Fig. 8. The impedance variation of the simulated cell depends on the electrode size.

These findings underscore the importance of optimizing electrode size and the spacing between electrodes, suggesting that within the 10 to 15 µm range, the impedance changes are most pronounced. Optimising these parameters can potentially enhance the sensitivity of impedance flow cytometry measurements. Further exploration of these optimised parameters holds promise for advancing studies in impedance-based cell detection and characterisation in microfluidic environments, contributing to the development of more effective methodologies for future research.

4.6. The influence of the frequency of excitation on the impedance signal

The frequency of excitation directly affects the complex impedance between electrodes. This study investigated the influence of excitation frequency on the performance of the proposed method. Under varying frequency conditions, both the resistive and reactive components of impedance were computed using the FEM model.

Building on the investigation of impedance variation in the proposed sensor structure, including both resistance and reactance, a detailed analysis was conducted across a frequency spectrum ranging from 1 kHz to 10 MHz. The Fig. 9 revealed substantial variations in resistance at distinct frequencies, with a significant reduction in resistance change as the frequency exceeded 90 kHz. Additionally, a marked alteration in reactance was observed, peaking between 500 and 600 kHz, followed by a gradual decrease beyond this range.

Based on the simulation findings, it is recommended to select an excitation frequency within the 500 to 600 kHz range for experimental purposes. This frequency range shows significant variations in both resistance and reactance components, providing an optimal balance between

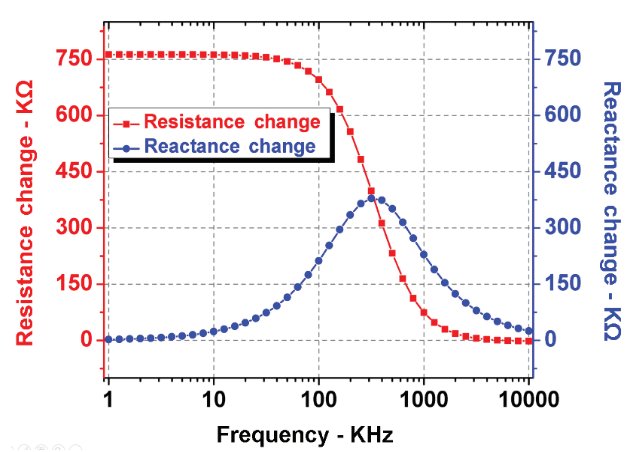

Fig. 9. The impact of frequency on the variations in resistance and reactance of the proposed sensing structure for detecting A549 cells.

sensitivity and precision. Moreover, the choice of excitation frequency should consider the performance of the integrated circuit, with careful attention to cost implications, especially at higher frequencies, in future experiments.

Beyond the technical aspects, this frequency range is ideal for cell detection in microchannels, extending to low-cost, portable devices used in biomedical settings. The optimised characteristics within this range enhance the microsensor's performance, making it suitable for practical and resource-efficient applications in biomedical fields. This highlights the multifaceted advantages of the proposed sensor structure, not only in its technical capabilities but also in its potential real-world applications.

5. Conclusions

This study investigated and structurally optimised a microfluidic chip featuring embedded coplanar electrodes to detect cells within a microfluidic channel using a complex impedance approach. A novel impedance analysis technique, which includes assessments of both resistance and reactance, was applied. The functionality of the sensing structure was validated through the FEM using COMSOL Multiphysics, with the Electric Current module defining scalar electric potential in a 3D model. The analysis results indicate that the sensitivity of the coplanar electrode design for detecting A549 cells is optimised when the electrode structure size falls within the 10 to 15 µm range. The simulation further explored the impact of cell size and position within the channel on impedance changes. This study not only validates the efficiency and feasibility of the proposed analysis method but also establishes a solid foundation for future experimental endeavours focused on detecting and enumerating biological cells for biomedical applications. The integration of coplanar electrodes in a microfluidic chip, as examined in this work, holds promise for enhanced cell detection sensitivity and sets the stage for advancing research in microfluidic-based cell analysis.

CRediT author statement

Van Phu Nguyen: Conceptualisation, Methodology, Data collection and analysis, Interpretation of results, Original draft preparation; Van-Anh Bui: Methodology, Design, Data collection, Interpretation of results; Thu Hang Nguyen: Data analysis, Interpretation of results, Revision; Trung Kien Do: Data collection and analysis; Van Thanh Pham: Interpretation of results, Original draft preparation; Thi Thanh Thuy Dang: Data analysis, Revision; Quang Loc Do: Conceptualisation, Methodology, Revision.

ACKNOWLEDGEMENTS

This research is funded by the University of Science, Vietnam National University - Hanoi under project number TN.23.07.

COMPETING INTERESTS

The authors declare that there is no conflict of interest regarding the publication of this article.

REFERENCES

[1] World Health Organization (2004), *The Global Burden of Disease: 2004 Update*, 146pp.

[2] D.R. Shopland, H.J. Eyre, T.F. Peachacek (1991), "Smoking-attributable cancer mortality in 1991: Is lung cancer now the leading cause of death among smokers in the United States?", *J. Natl. Cancer Inst.*, **83(16)**, pp.1142-1148, DOI: 10.1093/jnci/83.16.1142.

[3] J. Krüger, K. Singh, A. O'Neill, et al. (2002), "Development of a microfluidic device for fluorescence activated cell sorting", *J. Micromechanics Microengineering*, **12(4)**, DOI: 10.1088/0960-1317/12/4/324.

[4] World Health Organization (2009), *Guidelines for HIV Diagnosis and Monitoring of Antiretroviral Therapy*, https://apps.who.int/iris/bitstream/handle/10665/205162/B4375.pdf?sequence=1&isAllowed=y, accessed 15 October 2023.

[5] S. Zhu, X. Zhang, Z. Zhou, et al. (2021), "Microfluidic impedance cytometry for single-cell sensing: Review on electrode configurations", *Talanta*, **233**, DOI: 10.1016/j.talanta.2021.122571.

[6] C. Honrado, P. Bisegna, N.S. Swami, et al. (2021), "Single-cell microfluidic impedance cytometry: From raw signals to cell phenotypes using data analytics", *Lab Chip*, **21(1)**, pp.22-54, DOI: 10.1039/d0lc00840k.

[7] D.N. Hernández, J.R. Tosina, M. Min (2019), "Fundamentals, recent advances, and future challenges in bioimpedance devices for healthcare applications", *Journal of Sensors,* **2019**, DOI: 10.1155/2019/9210258.

[8] B.W. Dulken, M.T. Buckley, P.N. Negredo, et al. (2019), "Single-cell analysis reveals T cell infiltration in old neurogenic niches", *Nature*, **571(7764)**, pp.205-210, DOI: 10.1038/s41586-019-1362-5.

[9] H. Cho, J. Kim, H. Song, et al. (2018), "Microfluidic technologies for circulating tumor cell isolation", *Analyst*, **143(13)**, pp.2936-2970, DOI: 10.1039/C7AN01979C.

[10] R. Nasiri, A. Shamloo, J. Akbari, "Design of a hybrid inertial and magnetophoretic microfluidic device for CTCs separation from blood", *Micromachines*, **12(8)**, DOI: 10.3390/mi12080877.

[11] J. Chen, C.Y. Liu, X. Wang, et al. (2020), "3D printed microfluidic devices for circulating tumor cells (CTCs) isolation", *Biosens. Bioelectron.*, **150**, DOI: 10.1016/j.bios.2019.111900.

[12] N.D. Hai, V.Q. Tuan, D.Q. Loc, et al. (2016), "Differential C^4D sensor for conductive and non-conductive fluidic channel", *Microsyst. Technol.*, **22(10)**, pp.2511-2520, DOI: 10.1007/s00542-015-2586-4.

[13] L.Q. Do, T.T. Bui, H.T.T. Tran, et al. (2018), "Fluidic platform with embedded differential capacitively coupled contactless conductivity detector for micro-object sensing", *Int. J. Nanotechnol.*, **15(1-3)**, pp.24-38, DOI: 10.1504/IJNT.2018.089543.

[14] Y. Qiang, D. Dieujuste, J. Liu, et al. (2023), "Rapid electrical impedance detection of sickle cell vaso-occlusion in microfluidic device", *Biomed. Microdevices*, **25(3)**, DOI: 10.1007/s10544-023-00663-1.

[15] D. Dieujuste, Y. Qiang, E. Du (2021), "A portable impedance microflow cytometer for measuring cellular response to hypoxia", *Biotechnol. Bioeng.*, **118(10)**, pp.4041-4051, DOI: 10.1002/bit.27879.

[16] J. Liu, Y. Qiang, O. Alvarez, et al. (2018), "Electrical impedance microflow cytometry with oxygen control for detection of sickle cells", *Sensors Actuators B Chem.*, **255**, Pt. 2, pp.2392-2398, DOI: 10.1016/j.snb.2017.08.163.

[17] J. Chen, C. Xue, Y. Zhao, et al. (2015), "Microfluidic impedance flow cytometry enabling high-throughput single-cell electrical property characterization", *Int. J. Mol. Sci.*, **16(5)**, pp.9804-9830, DOI: 10.3390/ijms16059804.

[18] F. Caselli, P. Bisegna (2017), "Simulation and performance analysis of a novel high-accuracy sheathless microfluidic impedance cytometer with coplanar electrode layout", *Med. Eng. Phys.*, **48**, pp.81-89, DOI: 10.1016/j.medengphy.2017.04.005.

[19] J. Cottet, A. Kehren, H.V. Lintel, et al. (2019), "How to improve the sensitivity of coplanar electrodes and micro channel design in electrical impedance flow cytometry: A study", *Microfluid. Nanofluidics*, **23(1)**, DOI: 10.1007/s10404-018-2178-6.

[20] A. Farooq, N.Z. Butt, U. Hassan (2021), "Biochip with multi-planar electrodes geometry for differentiation of non-spherical bioparticles in a microchannel", *Sci. Rep.*, **11(1)**, DOI: 10.1038/s41598-021-91109-2.

[21] M.A. Warren, A. Shakouri, V.P. Peña, et al. (2023), "Development of a novel design of microfluidic impedance cytometry for improved sensitivity and cell identification", *ACS Omega*, **8(21)**, pp.18882-18890, DOI: 10.1021/acsomega.3c00797.

[22] F. Caselli, M. Shaker, L. Colella, et al. (2014), "Modeling, simulation, and performance evaluation of a novel microfluidic impedance cytometer for morphology-based cell discrimination", *J. Microelectromechanical Syst.*, **23(4)**, pp.785-794, DOI: 10.1109/JMEMS.2014.2325979.

[23] T. Tang, X. Liu, R. Kiya, et al. (2021), "Microscopic impedance cytometry for quantifying single cell shape", *Biosens. Bioelectron.*, **193**, DOI: 10.1016/j.bios.2021.113521.

[24] P.N. Van, A.B. Hoang, H.T. Thanh, et al. (2023), "Numerical calculation and analysis of a novel complex impedance sensing approach for in-flow droplet detection utilizing the C^4D technique", *Model. Simul. Mater. Sci. Eng.*, **31(7)**, DOI: 10.1088/1361-651X/acf513.

[25] H. Song, Y. Wang, J.M. Rosano, et al. (2013), "A microfluidic impedance flow cytometer for identification of differentiation state of stem cells", *Lab Chip*, **13(12)**, DOI: 10.1039/c3lc41321g.

[26] M. Kumar, S. Yadav, A. Kumar, et al. (2019), "MEMS impedance flow cytometry designs for effective manipulation of micro entities in health care applications", *Biosens. Bioelectron.*, **142**, DOI: 10.1016/j.bios.2019.111526.

[27] T. Sun, H. Morgan (2010), "Single-cell microfluidic impedance cytometry: A review", *Microfluid. Nanofluidics*, **8(4)**, pp.423-443, DOI: 10.1007/s10404-010-0580-9.

[28] K. Wang, Y. Zhao, D. Chen, et al. (2017), "The instrumentation of a microfluidic analyzer enabling the characterization of the specific membrane capacitance, cytoplasm conductivity, and instantaneous Young's modulus of single cells", *Int. J. Mol. Sci.*, **18(6)**, DOI: 10.3390/ijms18061158.

[29] M.E.G.D. Araùjo, L.A. Huber, T. Stasyk (2008), "Isolation of endocitic organelles by density gradient centrifugation", *Methods Mol. Biol.*, **424**, pp.317-331, DOI: 10.1007/978-1-60327-064-9_25.

[30] U. Lei, P.H. Sun, R. Pethig (2011), "Refinement of the theory for extracting cell dielectric properties from dielectrophoresis and electrorotation experiments", *Biomicrofluidics*, **5(4)**, DOI: 10.1063/1.3659282.

[31] A.D. Biasio, C. Cametti (2011), "On the dielectric relaxation of biological cell suspensions: The effect of the membrane electrical conductivity", *Colloids Surfaces B Biointerfaces*, **84(2)**, pp.433-441, DOI: 10.1016/j.colsurfb.2011.01.038.

[32] K. Asami, Y. Takahashi, S. Takashima (1990), "Frequency domain analysis of membrane capacitance of cultured cells (HeLa and myeloma) using the micropipette technique", *Biophys. J.*, **58(1)**, pp.143-148, DOI: 10.1016/S0006-3495(90)82360-2.

[33] D. Spencer, V. Hollis, H. Morgan (2014), "Microfluidic impedance cytometry of tumour cells in blood", *Biomicrofluidics*, **8(6)**, DOI: 10.1063/1.4904405.

[34] K.R. Foster, H.P. Schwan (1989), "Dielectric properties of tissues and biological materials: A critical review", *Crit. Rev. Biomed. Eng.*, **17(1)**, pp.25-104.

[35] Y. Zheng (2014), *Microfluidic Systems for High-Throughput Biophysical Characterization of Single Cells*, University of Toronto, 161pp.

[36] L.D. Quang, T.T. Bui, A.B. Hoang, et al. (2019), "Development of a passive capacitively coupled contactless conductivity detection (PC4D) sensor system for fluidic channel analysis toward point-of-care applications", *IEEE Sens. J.*, **19(15)**, pp.6371-6380, DOI: 10.1109/JSEN.2019.2908179.

[37] G. Mernier, E. Duqi, P. Renaud (2012), "Characterisation of a novel impedance cytometer design and its integration with lateral focusing by dielectrophoresis", *Lab Chip*, **12(21)**, DOI: 10.1039/c2lc40551b.

[38] F. Caselli, A.D. Ninno, R. Reale, et al. (2018), "A novel wiring scheme for standard chips enabling high-accuracy impedance cytometry", *Sensors Actuators B Chem.*, **256**, pp.580-589, DOI: 10.1016/j.snb.2017.10.113.

[39] J.W. Wang, M.H. Wang, L.S. Jang (2010), "Effects of electrode geometry and cell location on single-cell impedance measurement", *Biosens. Bioelectron.*, **25(6)**, pp.1271-1276, DOI: 10.1016/j.bios.2009.10.015.